ACS APPLIED MATERIALS & INTERFACES

Research Article

www.acsami.org

Selectively Sized Graphene-Based Nanopores for in Situ Single Molecule Sensing

Colin R. Crick,[†,§] Jasmine Y. Y. Sze,[†,§] Martin Rosillo-Lopez,[‡] Christoph G. Salzmann,[‡] and Joshua B. Edel*[,†]

[†]Department of Chemistry, Imperial College London, South Kensington Campus, London SW7 2AZ, United Kingdom

[‡]Department of Chemistry, University College London, 20 Gordon Street, London WC1H 0AJ, United Kingdom

Supporting Information

ABSTRACT: The use of nanopore biosensors is set to be extremely important in developing precise single molecule detectors and providing highly sensitive advanced analysis of biological molecules. The precise tailoring of nanopore size is a significant step toward achieving this, as it would allow for a nanopore to be tuned to a corresponding analyte. The work presented here details a methodology for selectively opening nanopores in real-time. The tunable nanopores on a quartz nanopipette platform are fabricated using the electroetching of a graphene-based membrane constructed from individual graphene nanoflakes (ø ~30 nm). The device design allows for in situ opening of the graphene membrane, from fully closed to fully opened (ø ~25 nm), a feature that has yet to be reported in the literature. The translocation of DNA is studied as the pore size is varied, allowing for subfeatures of DNA to be detected with slower DNA translocations at smaller pore sizes, and the ability to observe trends as the pore is opened. This approach opens the door to creating a device that can be target to detect specific analytes.

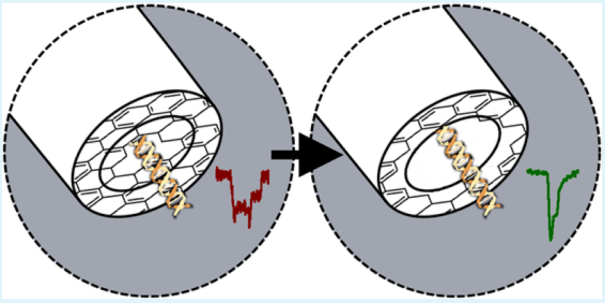

KEYWORDS: *nanopore, graphene, DNA, translocation, graphene nanoflake, size tuning*

INTRODUCTION

The development of comprehensive and efficient analysis techniques for biological molecules is a rapidly growing area of research.[1−4] A range of methods has recently been reported for the advanced analysis of single biological molecules.[5−8] Plausible outcomes in the future development of devices in this class would be to probe protein−nanopore interactions, protein−protein interactions, and eventually the ability to read the base pairs of DNA molecules by achieving higher spacial resolution and requiring only a single molecule to do so.[9,10] One category of these devices is nanopores, which are nanometer-sized holes that have been used in devices aimed toward detecting a range of molecules, including DNA and proteins.[11−14] The general principles of detection are grounded in passing biological molecules through a nanopore (translocation) by applying an electric field and observing experimental responses such as the ionic current. Further detection strategies also exist, including use of tunnelling currents, fluorescence, and surface-enhanced Raman spectroscopy, which can be carried out independently or employed as a synchronized detection platform.[15−17]

Major milestones for nanopore single molecule detection are the effective analysis of molecular components.[18,19] Many well-established nanopore systems in the scientific literature are capable of approximating molecular charge, size, and conformations.[20−22] The determination of further molecular properties has been reported, including the identification of molecular branching, in addition to probing the variations of molecular interaction with the nanopore surfaces.[18,23−25] These systems are dependent on the precise tailoring of nanopore size (diameter and length), in addition to the material from which it is constructed. The diameter of the nanopore must be large enough to allow the molecular analyte to fit through; however, a very large pore would result in an insignificant signal, making analysis increasingly difficult.[26] The material of the nanopore device also hugely influences the nature of interaction with the molecule as translocation occurs because an attraction or repulsion force may be present. This has been shown in many studies that examine nanopore surface functionalization.[27] The general principle of this approach is to cause an interaction to occur as the molecule translocates through the pore. This can be in an attractive force (including hydrogen bonds and van der Waals interactions) used to slow down the translocation speed, or a repulsive force (including large columbic forces), which may act to shrink the appreciable pore diameter.

The precise configuration of successful nanopore devices varies with respect to the specific analyte under investigation, in addition to the environmental conditions of the experiment

Received: July 10, 2015
Accepted: July 24, 2015
Published: July 24, 2015

DOI: 10.1021/acsami.5b06212
ACS Appl. Mater. Interfaces 2015, 7, 18188−18194

(i.e., solution concentrations, applied potentials, etc.).[28,29] A result of this is an aspiration for devices to be tunable so that a range of molecules can be used without the need for designing, fabricating, and testing a new device architecture. Electron beams, plasma etching, material deposition, and surface functionalization have been used to control the shapes and size of nanopores.[30−33] Materials including graphene have been utilized due to their high mechanical strength, which enables free-standing membranes to be formed to support a nanopore, in addition to widely reported low electrical noise and selectivity.[34−40] The graphene membranes used in the construction of these devices is exclusively single/multilayer graphene sheets suspended over voids. These sheets are then targeted for nanopore milling, primarily using electron and ion beams.

Previous literature reports the ability to select the size of nanopores supported on graphene membranes; however, the size of the pore must be determined before any biosensing experiment.[8,26,41−43] Electrochemical opening alongside DNA translocation experiments have been reported on molybdenum sulfide and silicon nitride free-standing membranes.[44−46] Recent reports have covered both the electrochemistry and the electrochemical etching of graphene membranes; however, the techniques involve a substantial amount of fabrication.[47,48] Relying upon cleanroom fabrication of nanopore devices and single layered graphene.

The work presented in this article aims to use multilayered graphene films to completely cover our nanopipette (see the Supporting Information for full experimental details). The aim of the experiments was to completely coat the pore at the end of the nanopipettes using water dispersed graphene nanoflakes (GNFs). The GNFs used in the experiment are small portions of single layered graphene (ø ∼30 nm) that are able to be dispersed in a solvent (Figure 1C).[49] Graphitic films are formed by annealing the GNF-coated nanopipettes in a vacuum oven. The nanopore coating is analyzed using ionic conductivity measurements. Alternating current (AC) is used to etch away the membrane material with the frequency applied potential and overall treatment length tuned for steady pore opening. The AC opening technique provides the opportunity for graphene membrane etching, electrical testing and DNA translocations to be performed without interruption. The translocation of DNA is carried out as the pores are opened, and any observed difference in DNA behavior is related to the effect of nanopore size. The reported technique aims to demonstrate precise in situ nanopore size control, which would be a vital tool in generating effective and broadly functioning nanopore devices.

The GNFs were produced by breaking down single-wall carbon nanotubes.[49] The aqueous GNF dispersions were prepared by dispersing 1, 1.5, and 3 mg of GNFs in 1.00 g of distilled water and gentle stirring. Quartz nanopipettes were engineered from microcapillaries (i.d., 0.5 mm; o.d., 1 mm). The pipettes were fabricated with a laser-based puller.[5,12,50] The pulling diameter generated pipettes with an average nanopore sizes of 25 nm (±2 nm) across 20 pipettes, which was estimated from pore conductance measurements (full details are available in the Supporting Information). These pipettes were then dipped into the GNF dispersions and withdrawn at a rate of 10 mm s^{-1}. The pipettes were air-dried for 10 min with the pipette tips pointing vertically downward. The pipettes were then placed in ceramic boats and placed inside a quartz tube attached to a high vacuum system and heated to 900 °C

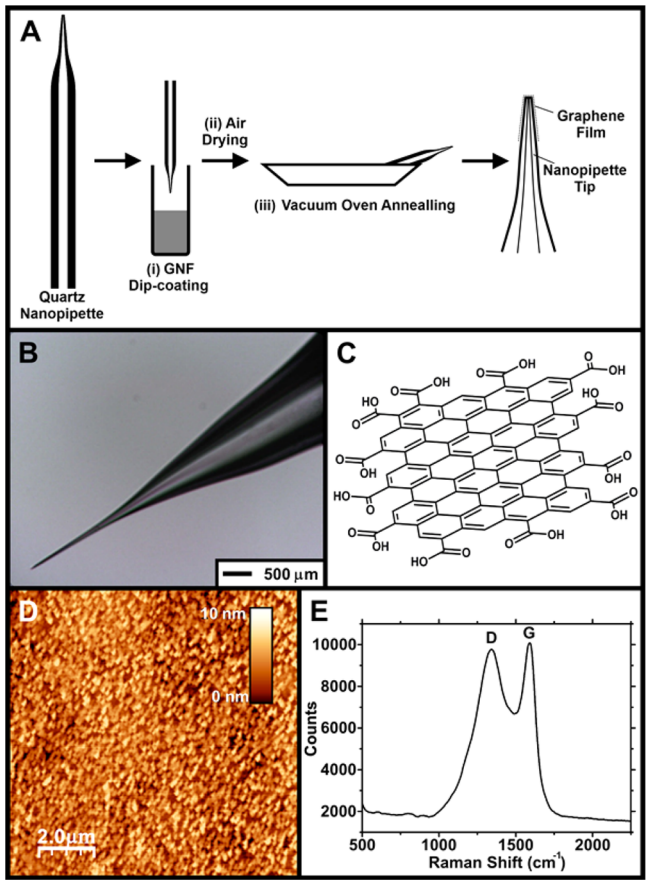

Figure 1. (A) Nanopipette coating schematic. Steps include (i) dip-coating pipettes into GNF solutions of various concentrations, (ii) leaving pipettes with tips pointing downward for 10 min of air drying, and (iii) vacuum annealing carried out at 900 °C and a pressure of ∼1.5 × 10^{-5} mbar. (B) Shows an optical image of the nanopipette (scale bar inset). (C) A cartoon of an individual small GNF. The size of each GNF is ∼30 nm, and the edges of the GNF are functionalized with carboxylic acid groups. (D) AFM image of a spin-coated GNFs annealed on a quartz substrate. The spin coating was carried out using a 1.5 mg mL^{-1} GNF solution, at a spin speed of 5000 rpm for 30 s. The individual features (ø ∼30 nm) are the annealed GNFs, the measured surface roughness indicates a multilayered arrangement (scale bar inset). (E) Raman spectrum of the annealed GNF film on quartz substrates. The characteristic D and G bands present in graphene are indicated on the spectrum.

over a period of 90 min (Figure 1A). Once cooled, the nanopipettes were sealed in airtight containers and only removed to be analyzed.

The characterization of GNF deposition has been previously reported and showed single sheet flakes of approximately 30 nm distributed homogeneously along substrate surfaces.[49] An illustration of an individual GNF is shown in Figure 1C. Deposition and the annealing of GNFs on quartz substrates were carried out to validate the resulting graphene materials. Uniform coatings of GNFs were achieved by spin-coating aqueous suspensions of various concentrations, which were subsequently annealed (Figure 1). The surface roughness of the deposited films was analyzed using AFM (Figure 1D). This showed the annealed GNFs (ø ∼30 nm) and surface features that were no taller than 10 nm. The surface roughness of the underlying substrate was also analyzed using AFM (Supporting Information, Figure S1). The maximum surface feature was

DOI: 10.1021/acsami.5b06212
ACS Appl. Mater. Interfaces 2015, 7, 18188−18194

measure as 5 nm, the additional surface roughness (+ 5 nm) caused by the graphene coating suggests a film consisting of multiple graphene layers. The resultant graphitic material was also analyzed using Raman spectroscopy (Figure 1E), which showed the D- and G-bands expected for a graphene film. The presence of an intense D-band indicates a film containing defects (i.e., not perfectly graphenic carbon). This imperfection is brought about by the "patchwork" nature of the resulting film composed of annealed GNFs. XPS analysis was carried out on the coatings (Supporting Information, Figure S2). In summary, the films were confirmed to be made up of defect-containing graphene, stacked into multiple layers (estimated at ∼5 nm).

The deposition of GNFs onto nanopipettes could not be achieved through a simple modification of a previously used GNF deposition technique (spin-coating or drop-casting). Dip-coating of the pipette tips (Figure 1) offered an adaptable coating method, which could be readily achieved. The spin coating experiments, carried out on flat substrates, were used to estimate the concentration required for a conformal coating. Various concentrations of GNF solutions were used to explore a variety coating conditions. Subsequent to dip-coating, the pipettes were left to air-dry for 10 min with their tips pointing downward, which demonstrated the most consistent nanopore coverage. Further orientations for pipettes drying were carried out (including pointing vertically upward and horizontally). However, this did not provide consistent nanopore coverage on the electrical measurement (i.e., the $I-V$ curve). When examined optically, the pipettes showed no coatings of GNF solutions with concentrations of 1.5 mg mL^{-1} or less; however there was a slight darkening of pipettes coated using 3 mg mL^{-1}. The annealed nanopipettes showed no change in overall appearance and shape (i.e., taper length, color, and angle of tip). The coatings on the pipettes were imaged using both SEM and TEM (Figure 2). SEM images of nanopipettes before and after the coating process show successful closing of the nanopore. TEM images of the pipette shaft show film thicknesses (∼3−4 nm) for the deposited material. A full experimental description is given in the Supporting Information.

The nanopore size was also estimated through conductivity measurements. The uncoated pipettes showed a conductance of 4.3 nS (±0.3 nS) at 0.1 M KCl. This is estimated to be a pore size of 25 nm (±2 nm) according to the model described by Steinbock et al.[51] The estimated pore diameters were also comparable to literature recently reported.[5] This value did not change upon undergoing the annealing process. Graphene deposition provided pore blockages for the majority of the treated pipettes at all concentrations, with the relative amounts of blockages increasing with concentration; 50% for 1 mg mL^{-1}, 84% for 1.5 mg mL^{-1}, and 93.5% for 3 mg mL^{-1}. The graphene-coated pipettes showed average conductance value (7 ± 0.8 pS) when electrically tested, indicating that the nanopore is closed. The pore opening process was aimed at steadily opening the membrane covering the nanopore. The protocol designed for opening uses a rapidly alternating current (±1.0 V at a frequency of 100 Hz), the pore opening was monitored by measuring current flow and subsequent $I-V$ measurements (Figure 3). This opening technique was selected because graphene materials have been shown to exhibit delamination and redox chemistry under an applied potential, while rapid reversal of applied potentials ensures a steady opening process.[52,53]

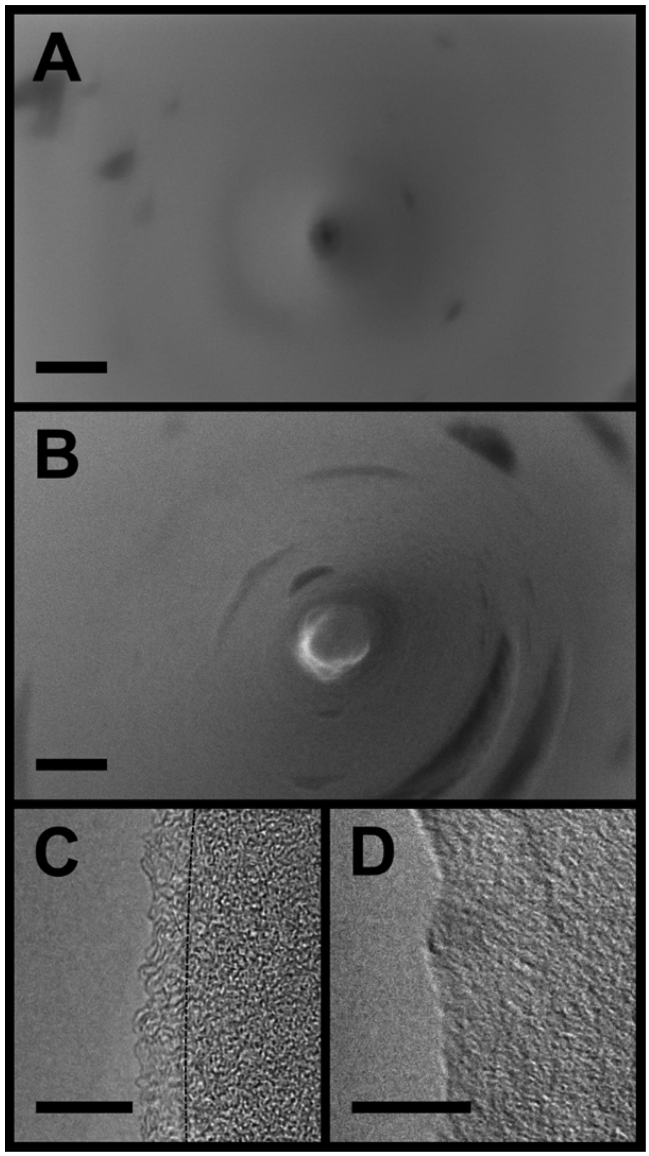

Figure 2. SEM images of (A) untreated and (B) GNF-coated nanopipettes. The untreated nanopipettes possess an average pore diameter of 25 nm. Scale bars in panels A and B are 100 nm. TEM images of (C) GNF coated and (D) untreated nanopipettes edges. The GNF-coated pipettes have a 3−4 nm coating of material on the surface. The dashed line on image C indicates the line of the underlying quartz of the pipet. Scale bars in panels C and D are 10 nm. The coated pipettes in the images are treated with 1.5 mg mL^{-1} of GNF solutions before being annealed.

Each opening sequence was carried out over a 200 s period. Typical current vs time traces are provided in the Supporting Information (Figure S3). The opening of multilayered graphene films was consistent for each concentration of GNF solutions used for dip coating. The higher concentration solutions, however, gave films that required a greater number of opening sequences to increase the pore size. The pipettes coated with 1.5 mg mL^{-1} were found to be optimal for opening experiments, providing a large amount of blocked pores while also providing steady opening for detecting DNA molecules. The average ratio of pore opening (final pore diameter/untreated pore diameter) for these pipettes was ∼0.7, which provided a large range of pore sizes as the electroetching progressed. The lower proportion of blocked pipettes at lower

DOI: 10.1021/acsami.5b06212
ACS Appl. Mater. Interfaces 2015, 7, 18188−18194

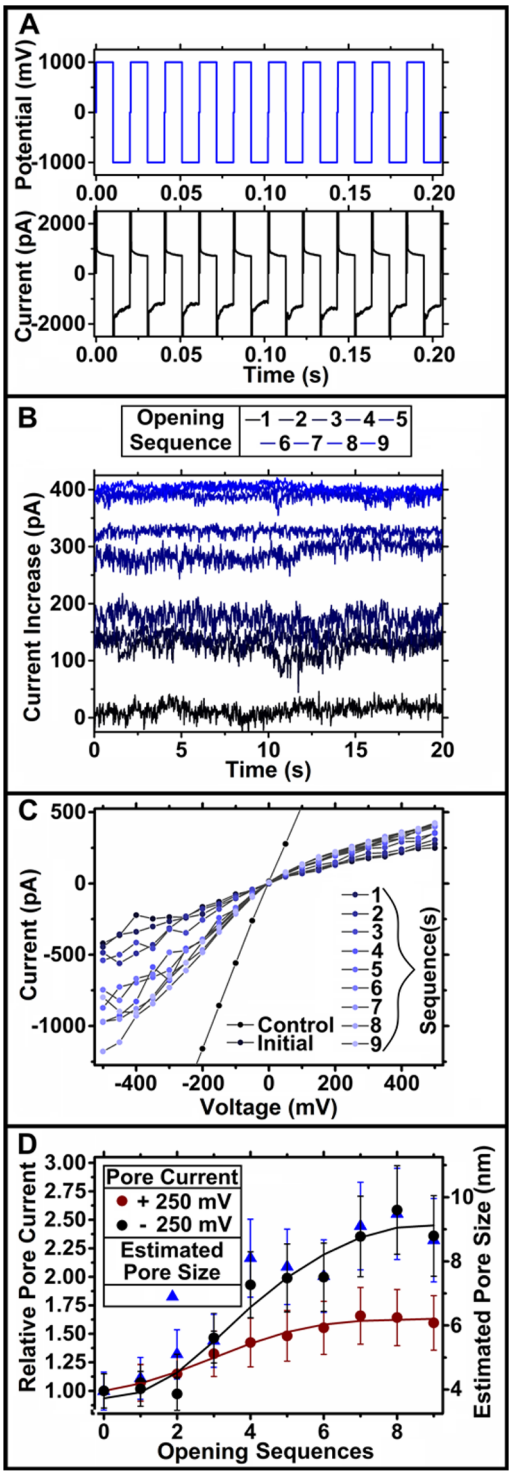

Figure 3. (A) Plot of the repeating square wave potential applied to the multilayered graphene membranes. A corresponding current trace from a nanopore coated using 1.5 mg mL^{-1} of GNF solution is shown. (B) Shows the current increase/time trace for the first 20 s of each pore opening sequences for the same pipette, generated by using the average positive current flow (shown in 3A, from ~0−10 ms in the square wave cycle). The trend shows a general increase in current after each opening sequence. (C) Nanopipette *I*−*V* plots after subsequent nanopore opening sequences. The pore opens from completely closed to a final estimate size of 8.7 nm after 9 sequences. (D) Plot of the pore current at positive and negative potentials as the pore is opened. The corresponding estimated pore size is also shown.

concentration is due to incomplete coverage achieved in the dip-coating process, with this principle extended to more substantial GNF coating achieved at higher solution concentrations. The greater effort required to open the graphene films formed using higher GNF solution concentration was caused by the resultant carbonized coating being thicker and more consistent around the nanopipette. The pore opening process, could be primarily monitored through the current allowed to pass during the AC opening sequence (Figure 3A). The mean current flow would increase as the opening sequence was carried out (Figure 3B). This current flow is a direct indicator of the pore size, allowing for progressive monitoring as the opening sequence was applied. This was also used to gauge if a pore had reached its maximal size, with no increase observed throughout the sequence. After each opening sequence, *I*−*V* measurements were taken to more accurately estimate the pore size (Figure 3C). Pipette coatings carried out using 1.5 mg mL^{-1} could be opened with relative ease. Consecutive opening sequences resulted in the opening of the pore from fully closed to an estimated 9 nm in 9 sequences (Figure 3D). The thicker coatings generated by using 3 mg mL^{-1} were harder to open (Supporting Information, Figure S4). The fully closed pores were commonly not open at all by numerous opening sequences. An optimal opening rate of 1.2 (±0.17) nm per sequence was achieved using an initial GNF solution of 1.5 mg mL^{-1}, this allowed for the size of the nanopore to be precisely tuned to detect specific analyte.

The mechanism for the membrane opening could follow two main mechanisms, either via atom-by-atom removal or by sporadic flaking of the membrane, brought about by the electroetching of the graphene.[52,53] The opening rate of the multilayered graphene membranes is somewhat consistent between opening sequences (Figure 3D). However, some fluctuation is seen in the current increase during the opening sequences (Figure 3B). Current flow was stable upon completion of the opening sequences, with similar baseline noise levels observed for both GNF-treated and untreated nanopipettes (Supporting Information, Figure S5). Opening occurring through an atom-by-atom removal would provide linear increases during the opening sequence. As this is not the case, a mechanism whereby masses of the graphene membrane is removed intermittently is most likely. However, pore opening data does not indicate the precise nature of this.

The translocation behavior of DNA was then studied, the aim was to monitor variations in translocation behavior as the graphene membrane was opened. All of the reported DNA translocations were carried out using one type of DNA (10 kbp). With full characterization of the translocation behavior of the DNA carried out on untreated pipettes. Both the DNA concentration and ionic strength of the solution were kept constant throughout all reported experiments, however the potential applied to drive the translocations was varied. This change in applied potential provides differences in observed translocations (Figure 4). The current−time traces show a positive spike in current as the DNA passes through due to the extra charge carried by the DNA molecule. The features of each spike is characteristic of the pore properties, in addition to the conformation of the DNA as it passes through the nanopore (Figure 4A). The most important features of these traces are the dwell time (the total time for a translocation event), peak amplitude (the maximum height of a translocation peak from the baseline) and charge (the integrated area underneath the plotted translocation event). Detailed analysis of multiple

DOI: 10.1021/acsami.5b06212
ACS Appl. Mater. Interfaces 2015, 7, 18188−18194

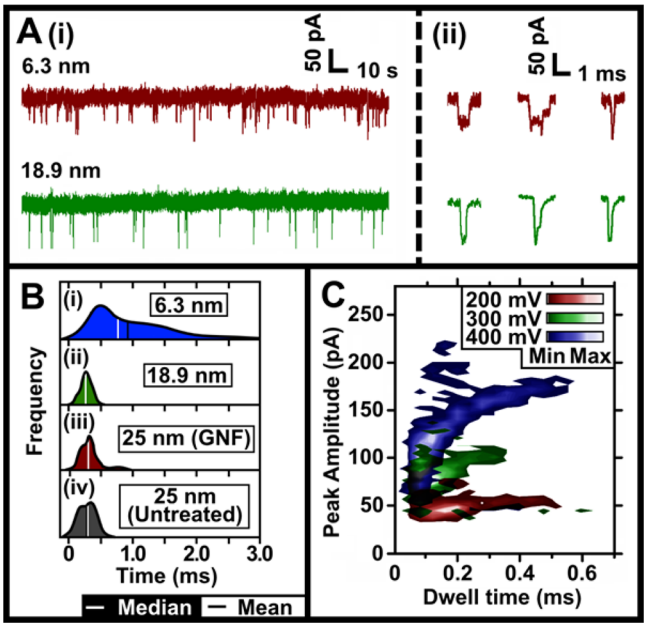

Figure 4. Translocation data for 10 kbp DNA through nanopores treated with multilayered graphene membrane. (A) Current−time traces of DNA translocations through a GNF coated nanopores. Individual translocation events are also shown. (B) "Half-violin" plots showing the average dwell time at different size of pore at various stages of opening, the overall trend shows the dwell time decreases as the pore diameter increases. (C) Translocation data from pipette membranes fabricated using an initial 1.5 mg mL^{-1} GNF solution. The data shows the separation of DNA conformations as the applied potential is varied. All of the applied potentials have translocation events that occur at ∼50 pA, this splits into two populations for both the 300 mV (∼75 pA) and 400 mV (∼125 pA) cases. The estimated pore size for this was ∼22 nm.

translocation events reveals typical values of 0.37 (±0.02) ms, 59.3 (±3.6) pA, and 17.1 (±2.17) fA for dwell time, peak amplitude, and charge, respectively, at an applied potential of 300 mV, using untreated nanopipettes.

The translocation of DNA was carried out in conjunction with the pore-opening experiments described above, with translocations attempted at each stage of opening process. The DNA solution used in each pipette was introduced using a MicroFil needle, the same DNA solution was used for all steps of opening and DNA sensing and was not exchanged at any point. The tip of the MicroFil needle was thin enough to reach the tip of the pipette, and so no air was trapped inside upon filling. The partially open pores were then examined for differences in translocation behavior. The current flow through the pore during translocations was found to be stable for the vast majority of nanopores at the various stages of opening. This made the observation of translocation events straightforward (Figure 4A). The systematic analysis of the coated pipettes found that there were no observed translocations using pipettes with pore sizes less than 6.3 nm; however, there were bumping events at 5.52 nm; alternatively, this might be due to the GNF flakes interacting with the DNA near the pore entrance. Additionally, fully opened nanopipettes showed moderate differences in translocation behavior compared to measurements taken using noncoated pipettes (Figure 4B). This indicates that there was some interaction between the graphene coating and translocating DNA once the pipettes were fully opened. The major differences between these two cases include an increased average dwell time (from 0.37 to 0.83 ms) at 300 mV and increased the distribution of dwell times. These values compare well with reported nanopore devices fabricated from graphene membranes.[54,55] As the pore size was opened past 6.3 nm in size, translocations were observed. At these initially small nanopore sizes, the translocation events had longer dwell times (Figure 4B). This longer dwell time is caused by a range of factors, including the effect of confining the translocation volume, in addition to chemical interaction between the DNA and the graphene membrane. The reduction in pore size increases the energy barrier for DNA translocation. Another effect of the small pore sizes is that the DNA must unravel in order to translocate; this conformation intrinsically has a longer translocation time compared to a more constricted conformation. Additionally, the DNA may interact significantly with the graphene coating as it passes through. The electrochemical process used to open the pore may cause hydrophilic groups appearing at the surface, and these groups would attract the DNA molecules toward the membrane material, an effect that would be greatest at smaller pore sizes.[56] The overall dwell time is reduced as the nanopore is fully opened, which supports this concept.

DNA translocation detection depends heavily on the size of the nanopore used.[28,29] It was found throughout the experiments that specific nanopore sizes lead to atypical observations of DNA behavior. This is exemplified by an example shown in Figure 4C. The particular nanopore was fabricated using an initial 1.5 mg mL^{-1} GNF, and the pore was opened to an estimated diameter of 22 nm. At an applied potential of 200 mV, a single DNA population was observed, indicating an unfolded state of the molecules passed through the pore; however, second populations appeared when voltage was increased to both 300 and 400 mV. Usually, we would expect this is due to different conformations of the DNA passing the pore; however, the excluded charge (integrated current area per translocation event) values were very similar to 200 mV (5.43 ± 2.2 fAs), only increased by 1.5 fA as the voltage increased by 100 mV, indicating that other factors are affected. As discussed in the Supporting Information, the uncoated nanopipette at 25 nm had an excluded charge of 13.95 ± 3.01 fAs at 200 mV, which is in agreement with other literature.[12] We hypothesize that this is due to the shape of the opening pore. Under typical circumstances, the nanopore would be thought to be circular; however, the irregular multilayer graphene coating may have caused a noncircular opening in this case. As the size estimations are modeled on circular pores, this behavior may be caused by a "letter box" shaped pore, confining the translocation in one dimension, hence affecting the time of DNA passage through the pore.

The electrostatic interaction of the mobile ions with the nanopore surface charge is a factor that plays an important role in translocation behavior in these devices to determine the device selectivity and rectification.[57] The untreated pipette has a rectification ratio of 1.83 ± 0.3 at 0.1 M KCl at pH 8.0, which is consistent with other literature.[58,59] The rectification ratio indicates that the K^+ ions flow more freely at negative applied potentials than at positive potentials. The modified pipette at the same pH has a rectification ratio of 2.67 ± 0.52, which is slightly higher than that of the untreated nanopipette. This further enhances the selectivity and the negatively charged surface on the nanopipette. This may be caused by a number of factors, including that as the graphene coating is electro-etched and opened, a functionality such as a negative carboxylate

DOI: 10.1021/acsami.5b06212
ACS Appl. Mater. Interfaces 2015, 7, 18188−18194

group may be added to the surface. This carboxylate group could have respond to the electric field, which then changes the effective diameter of the pore and may even close it, resulting in higher rectification ratio.[60] Other characteristics that may contribute to surface charge effects include the electron density of the graphene coating.[26]

CONCLUSION

The present work demonstrates the in situ controlled opening of nanopores via electroetching. The multilayered graphene membranes are shown to be able to provide nanopores of any size between that of complete closure and fully opened pores. Through this, we have achieved in situ nanopore opening, allowing for the size to be varied as translocation experiments are carried out. The nanopipette devices demonstrate differences in DNA translocations, with small pores demonstrating very different dwell times. These properties are facilitated by a targeted coating using GNFs (30 nm in diameter) to coat the nanopipette devices with a 25 nm diameter nanopore. The GNF films were annealed to form fully characterized graphene films. The film thickness was optimized to provide consistent coating and ease of opening. This was obtained by using a 1.5 mg mL^{-1} GNF solution for dip-coating, which provided a 3−4 nm thick film. Targeted nanopore opening will avoid the necessity to design and fabricate new nanopore architectures, as it is possible to tune the pore size to the analyte being probed. The technology reported also provides key benefits with respect to other reported techniques, such that the nanopipette fabrication and coating technique are both readily achieved and do not require any cleanroom fabrication. Use of graphene membranes is also compatible with surface functionalization and would provide a platform where surface chemistry could be tuned to further explore a molecule of interest.

ASSOCIATED CONTENT

Supporting Information

The Supporting Information is available free of charge on the ACS Publications website at DOI: 10.1021/acsami.5b06212.

Experimental details, further materials, and electrical characterization (PDF)

AUTHOR INFORMATION

Corresponding Author

*Email: joshua.edel@imperial.ac.uk.

Author Contributions

[§]These authors contributed equally to the manuscript. The manuscript was written through contributions of all authors. All authors have given approval to the final version of the manuscript.

Notes

The authors declare no competing financial interest.

ACKNOWLEDGMENTS

This work was supported in part by an ERC starting investigator grant (NanoP 279818) and BBSRC grant (BB/L017865/1) to J.B.E. C.R.C. acknowledges support from the Ramsay Memorial Trust, and C.G.S. acknowledges support from the Royal Society (UF100144).

REFERENCES

(1) Fan, X.; White, I. M.; Shopova, S. I.; Zhu, H.; Suter, J. D.; Sun, Y. Sensitive Optical Biosensors for Unlabeled Targets: A Review. *Anal. Chim. Acta* **2008**, *620* (1−2), 8−26.
(2) Ronkainen, N. J.; Halsall, H. B.; Heineman, W. R. Electrochemical Biosensors. *Chem. Soc. Rev.* **2010**, *39* (5), 1747−1763.
(3) Turner, A. P. F. Biosensors: Sense and Sensibility. *Chem. Soc. Rev.* **2013**, *42* (8), 3184−3196.
(4) Tamayo, J.; Kosaka, P. M.; Ruz, J. J.; San Paulo, Á.; Calleja, M. Biosensors Based on Nanomechanical Systems. *Chem. Soc. Rev.* **2013**, *42* (3), 1287−1311.
(5) Ivanov, A. P.; Actis, P.; Jönsson, P.; Klenerman, D.; Korchev, Y.; Edel, J. B. On-Demand Delivery of Single DNA Molecules Using Nanopipets. *ACS Nano* **2015**, *9* (4), 3587−3595.
(6) Guo, X. Single-Molecule Electrical Biosensors Based on Single-Walled Carbon Nanotubes. *Adv. Mater.* **2013**, *25* (25), 3397−3408.
(7) Okumoto, S.; Jones, A.; Frommer, W. B. Quantitative Imaging with Fluorescent Biosensors. *Annu. Rev. Plant Biol.* **2012**, *63* (1), 663−706.
(8) Maragò, O. M.; Jones, P. H.; Gucciardi, P. G.; Volpe, G.; Ferrari, A. C. Optical Trapping and Manipulation of Nanostructures. *Nat. Nanotechnol.* **2013**, *8* (11), 807−819.
(9) Lei, J.; Ju, H. Signal Amplification Using Functional Nanomaterials for Biosensing. *Chem. Soc. Rev.* **2012**, *41* (6), 2122−2134.
(10) Branton, D.; Deamer, D. W.; Marziali, A.; Bayley, H.; Benner, S. A.; Butler, T.; Di Ventra, M.; Garaj, S.; Hibbs, A.; Huang, X.; Jovanovich, S. B.; Krstic, P. S.; Lindsay, S.; Ling, X. S.; Mastrangelo, C. H.; Meller, A.; Oliver, J. S.; Pershin, Y. V.; Ramsey, J. M.; Riehn, R.; Soni, G. V.; Tabard-Cossa, V.; Wanunu, M.; Wiggin, M.; Schloss, J. A. The Potential and Challenges of Nanopore Sequencing. *Nat. Biotechnol.* **2008**, *26* (10), 1146−1153.
(11) Crick, C. R.; Albella, P.; Ng, B.; Ivanov, A. P.; Roschuk, T.; Cecchini, M. P.; Bresme, F.; Maier, S. A.; Edel, J. B. Precise Attoliter Temperature Control of Nanopore Sensors Using a Nanoplasmonic Bullseye. *Nano Lett.* **2015**, *15* (1), 553−559.
(12) Gong, X.; Patil, A. V.; Ivanov, A. P.; Kong, Q.; Gibb, T.; Dogan, F.; deMello, A. J.; Edel, J. B. Label-Free In-Flow Detection of Single DNA Molecules Using Glass Nanopipettes. *Anal. Chem.* **2014**, *86* (1), 835−841.
(13) Li, J.; Gershow, M.; Stein, D.; Brandin, E.; Golovchenko, J. A. DNA Molecules and Configurations in a Solid-State Nanopore Microscope. *Nat. Mater.* **2003**, *2* (9), 611−615.
(14) Miles, B. N.; Ivanov, A. P.; Wilson, K. A.; Doğan, F.; Japrung, D.; Edel, J. B. Single Molecule Sensing with Solid-State Nanopores: Novel Materials, Methods, and Applications. *Chem. Soc. Rev.* **2012**, *42* (1), 15−28.
(15) Ivanov, A. P.; Instuli, E.; McGilvery, C. M.; Baldwin, G.; McComb, D. W.; Albrecht, T.; Edel, J. B. DNA Tunneling Detector Embedded in a Nanopore. *Nano Lett.* **2011**, *11* (1), 279−285.
(16) Pitchford, W. H.; Kim, H.-J.; Ivanov, A. P.; Kim, H.-M.; Yu, J.-S.; Leatherbarrow, R. J.; Albrecht, T.; Kim, K.-B.; Edel, J. B. Synchronized Optical and Electronic Detection of Biomolecules Using a Low Noise Nanopore Platform. *ACS Nano* **2015**, *9* (2), 1740−1748.
(17) Cecchini, M. P.; Wiener, A.; Turek, V. A.; Chon, H.; Lee, S.; Ivanov, A. P.; McComb, D. W.; Choo, J.; Albrecht, T.; Maier, S. A.; Edel, J. B. Rapid Ultrasensitive Single Particle Surface-Enhanced Raman Spectroscopy Using Metallic Nanopores. *Nano Lett.* **2013**, *13* (10), 4602−4609.
(18) Singer, A.; Rapireddy, S.; Ly, D. H.; Meller, A. Electronic Barcoding of a Viral Gene at the Single-Molecule Level. *Nano Lett.* **2012**, *12* (3), 1722−1728.
(19) Brème, C.; Heslot, F. Mapping of Single-Base Differences between Two DNA Strands in a Single Molecule Using Holliday Junction Nanomechanics. *PLoS One* **2013**, *8* (2), e55154.
(20) Han, C.; Hou, X.; Zhang, H.; Guo, W.; Li, H.; Jiang, L. Enantioselective Recognition in Biomimetic Single Artificial Nanochannels. *J. Am. Chem. Soc.* **2011**, *133* (20), 7644−7647.

DOI: 10.1021/acsami.5b06212
ACS Appl. Mater. Interfaces 2015, 7, 18188−18194

(21) Niedzwiecki, D. J.; Iyer, R.; Borer, P. N.; Movileanu, L. Sampling a Biomarker of the Human Immunodeficiency Virus across a Synthetic Nanopore. *ACS Nano* **2013**, *7* (4), 3341−3350.
(22) Ali, M.; Neumann, R.; Ensinger, W. Sequence-Specific Recognition of DNA Oligomer Using Peptide Nucleic Acid (PNA)-Modified Synthetic Ion Channels: PNA/DNA Hybridization in Nanoconfined Environment. *ACS Nano* **2010**, *4* (12), 7267−7274.
(23) Kowalczyk, S. W.; Hall, A. R.; Dekker, C. Detection of Local Protein Structures along DNA Using Solid-State Nanopores. *Nano Lett.* **2010**, *10* (1), 324−328.
(24) Fanzio, P.; Mussi, V.; Menotta, M.; Firpo, G.; Repetto, L.; Guida, P.; Angeli, E.; Magnani, M.; Valbusa, U. Selective Protein Detection with a dsLNA-Functionalized Nanopore. *Biosens. Bioelectron.* **2015**, *64*, 219−226.
(25) Ali, M.; Schiedt, B.; Neumann, R.; Ensinger, W. Biosensing with Functionalized Single Asymmetric Polymer Nanochannels. *Macromol. Biosci.* **2010**, *10* (1), 28−32.
(26) Liu, K.; Feng, J.; Kis, A.; Radenovic, A. Atomically Thin Molybdenum Disulfide Nanopores with High Sensitivity for DNA Translocation. *ACS Nano* **2014**, *8* (3), 2504−2511.
(27) Luan, B.; Stolovitzky, G.; Martyna, G. Slowing and Controlling the Translocation of DNA in a Solid-State Nanopore. *Nanoscale* **2012**, *4* (4), 1068−1077.
(28) Sauer-Budge, A. F.; Nyamwanda, J. A.; Lubensky, D. K.; Branton, D. Unzipping Kinetics of Double-Stranded DNA in a Nanopore. *Phys. Rev. Lett.* **2003**, *90* (23), 238101.
(29) Mara, A.; Siwy, Z.; Trautmann, C.; Wan, J.; Kamme, F. An Asymmetric Polymer Nanopore for Single Molecule Detection. *Nano Lett.* **2004**, *4* (3), 497−501.
(30) Choi, S. S.; Park, M.-J.; Yamaguchi, T.; Kim, S.-I.; Park, K.-J.; Park, N. K. Fabrication of Nanopore on Pyramid. *Appl. Surf. Sci.* **2014**, *310*, 196−203.
(31) Li, N.; Yu, S.; Harrell, C. C.; Martin, C. R. Conical Nanopore Membranes. Preparation and Transport Properties. *Anal. Chem.* **2004**, *76* (7), 2025−2030.
(32) Chen, Z.; Jiang, Y.; Dunphy, D. R.; Adams, D. P.; Hodges, C.; Liu, N.; Zhang, N.; Xomeritakis, G.; Jin, X.; Aluru, N. R.; Gaik, S. J.; Hillhouse, H. W.; Jeffrey Brinker, C. DNA Translocation through an Array of Kinked Nanopores. *Nat. Mater.* **2010**, *9* (8), 667−675.
(33) Meng, H.; Xue, M.; Xia, T.; Zhao, Y.-L.; Tamanoi, F.; Stoddart, J. F.; Zink, J. I.; Nel, A. E. Autonomous in Vitro Anticancer Drug Release from Mesoporous Silica Nanoparticles by pH-Sensitive Nanovalves. *J. Am. Chem. Soc.* **2010**, *132* (36), 12690−12697.
(34) Freedman, K. J.; Ahn, C. W.; Kim, M. J. Detection of Long and Short DNA Using Nanopores with Graphitic Polyhedral Edges. *ACS Nano* **2013**, *7* (6), 5008−5016.
(35) Garaj, S.; Liu, S.; Golovchenko, J. A.; Branton, D. Molecule-Hugging Graphene Nanopores. *Proc. Natl. Acad. Sci. U.S.A.* **2013**, *110* (30), 12192−12196.
(36) Wells, D. B.; Belkin, M.; Comer, J.; Aksimentiev, A. Assessing Graphene Nanopores for Sequencing DNA. *Nano Lett.* **2012**, *12* (8), 4117−4123.
(37) Schneider, G. F.; Xu, Q.; Hage, S.; Luik, S.; Spoor, J. N. H.; Malladi, S.; Zandbergen, H.; Dekker, C. Tailoring the Hydrophobicity of Graphene for Its Use as Nanopores for DNA Translocation. *Nat. Commun.* **2013**, *4*, 2619.
(38) Nam, S.; Choi, I.; Fu, C.; Kim, K.; Hong, S.; Choi, Y.; Zettl, A.; Lee, L. P. Graphene Nanopore with a Self-Integrated Optical Antenna. *Nano Lett.* **2014**, *14* (10), 5584−5589.
(39) Shan, Y. P.; Tiwari, P. B.; Krishnakumar, P.; Vlassiouk, I.; Li, W. Z.; Wang, X. W.; Darici, Y.; Lindsay, S. M.; Wang, H. D.; Smirnov, S.; He, J. Surface Modification of Graphene Nanopores for Protein Translocation. *Nanotechnology* **2013**, *24* (49), 495102.
(40) Liu, S.; Zhao, Q.; Xu, J.; Yan, K.; Peng, H.; Yang, F.; You, L.; Yu, D. Fast and Controllable Fabrication of Suspended Graphene Nanopore Devices. *Nanotechnology* **2012**, *23* (8), 085301.
(41) Shankla, M.; Aksimentiev, A. Conformational Transitions and Stop-and-Go Nanopore Transport of Single-Stranded DNA on Charged Graphene. *Nat. Commun.* **2014**, *5*, 5171.
(42) Qiu, W.; Skafidas, E. Detection of Protein Conformational Changes with Multilayer Graphene Nanopore Sensors. *ACS Appl. Mater. Interfaces* **2014**, *6* (19), 16777−16781.
(43) Walker, M. I.; Weatherup, R. S.; Bell, N. A. W.; Hofmann, S.; Keyser, U. F. Free-Standing Graphene Membranes on Glass Nanopores for Ionic Current Measurements. *Appl. Phys. Lett.* **2015**, *106* (2), 023119.
(44) Feng, J.; Liu, K.; Graf, M.; Lihter, M.; Bulushev, R. D.; Dumcenco, D.; Alexander, D. T. L.; Krasnozhon, D.; Vuletic, T.; Kis, A.; Radenovic, A. Electrochemical Reaction in Single Layer MoS2: Nanopores Opened Atom by Atom. *Nano Lett.* **2015**, *15* (5), 3431−3438.
(45) Briggs, K.; Charron, M.; Kwok, H.; Le, T.; Chahal, S.; Bustamante, J.; Waugh, M.; Tabard-Cossa, V. Kinetics of Nanopore Fabrication during Controlled Breakdown of Dielectric Membranes in Solution. *Nanotechnology* **2015**, *26* (8), 084004.
(46) Kwok, H.; Briggs, K.; Tabard-Cossa, V. Nanopore Fabrication by Controlled Dielectric Breakdown. *PLoS One* **2014**, *9* (3), e92880.
(47) Banerjee, S.; Shim, J.; Rivera, J.; Jin, X.; Estrada, D.; Solovyeva, V.; You, X.; Pak, J.; Pop, E.; Aluru, N.; Bashir, R. Electrochemistry at the Edge of a Single Graphene Layer in a Nanopore. *ACS Nano* **2013**, *7* (1), 834−843.
(48) Kuan, A. T.; Lu, B.; Xie, P.; Szalay, T.; Golovchenko, J. A. Electrical Pulse Fabrication of Graphene Nanopores in Electrolyte Solution. *Appl. Phys. Lett.* **2015**, *106* (20), 203109.
(49) Salzmann, C. G.; Nicolosi, V.; Green, M. L. H. Edge-Carboxylated Graphene Nanoflakes from Nitric Acid Oxidised Arc-Discharge Material. *J. Mater. Chem.* **2009**, *20* (2), 314−319.
(50) Sze, J. Y. Y.; Kumar, S.; Ivanov, A. P.; Oh, S.-H.; Edel, J. B. Fine Tuning of Nanopipettes Using Atomic Layer Deposition for Single Molecule Sensing. *Analyst* **2015**, *140* (14), 4828−4834.
(51) Steinbock, L. J.; Lucas, A.; Otto, O.; Keyser, U. F. Voltage-Driven Transport of Ions and DNA through Nanocapillaries. *Electrophoresis* **2012**, *33* (23), 3480−3487.
(52) Ambrosi, A.; Chua, C. K.; Bonanni, A.; Pumera, M. Electrochemistry of Graphene and Related Materials. *Chem. Rev.* **2014**, *114* (14), 7150−7188.
(53) Yang, X.; Peng, H.; Xie, Q.; Zhou, Y.; Liu, Z. Clean and Efficient Transfer of CVD-Grown Graphene by Electrochemical Etching of Metal Substrate. *J. Electroanal. Chem.* **2013**, *688*, 243−248.
(54) Merchant, C. A.; Healy, K.; Wanunu, M.; Ray, V.; Peterman, N.; Bartel, J.; Fischbein, M. D.; Venta, K.; Luo, Z.; Johnson, A. T. C.; Drndić, M. DNA Translocation through Graphene Nanopores. *Nano Lett.* **2010**, *10* (8), 2915−2921.
(55) Banerjee, S.; Wilson, J.; Shim, J.; Shankla, M.; Corbin, E. A.; Aksimentiev, A.; Bashir, R. Slowing DNA Transport Using Graphene−DNA Interactions. *Adv. Funct. Mater.* **2015**, *25* (6), 936−946.
(56) Yuan, W.; Zhou, Y.; Li, Y.; Li, C.; Peng, H.; Zhang, J.; Liu, Z.; Dai, L.; Shi, G. The Edge- and Basal-Plane-Specific Electrochemistry of a Single-Layer Graphene Sheet. *Sci. Rep.* **2013**, *3*, 2248.
(57) Umehara, S.; Pourmand, N.; Webb, C. D.; Davis, R. W.; Yasuda, K.; Karhanek, M. Current Rectification with Poly-L-Lysine-Coated Quartz Nanopipettes. *Nano Lett.* **2006**, *6* (11), 2486−2492.
(58) Wei, C.; Bard, A. J.; Feldberg, S. W. Current Rectification at Quartz Nanopipet Electrodes. *Anal. Chem.* **1997**, *69* (22), 4627−4633.
(59) Sa, N.; Baker, L. A. Experiment and Simulation of Ion Transport through Nanopipettes of Well-Defined Conical Geometry. *J. Electrochem. Soc.* **2013**, *160* (6), H376−H381.
(60) Siwy, Z.; Gu, Y.; Spohr, H. A.; Baur, D.; Wolf-Reber, A.; Spohr, R.; Apel, P.; Korchev, Y. E. Rectification and Voltage Gating of Ion Currents in a Nanofabricated Pore. *Europhys. Lett.* **2002**, *60* (3), 349.

DOI: 10.1021/acsami.5b06212
ACS Appl. Mater. Interfaces 2015, 7, 18188−18194